1-1-2011

Micro-cracks informed damage models for brittle solids

Xiaodan Ren
Tongji University

Jiun-Shyan Chen
University of California - Los Angeles, jschen@seas.ucla.edu

Jie Li
Tongji University

T. R. Slawson
US Army Engineer Research and Development Center

M. J. Roth
US Army Engineer Research and Development Center

ARTICLE IN PRESS

International Journal of Solids and Structures xxx (2011) xxx–xxx

Contents lists available at ScienceDirect

International Journal of Solids and Structures

journal homepage: www.elsevier.com/locate/ijsolstr

Micro-cracks informed damage models for brittle solids

Xiaodan Ren [a], Jiun-Shyan Chen [b,*], Jie Li [a], T.R. Slawson [c], M.J. Roth [c]

[a] School of Civil Engineering, Tongji University, 1239 Siping Road, Shanghai 200092, China
[b] Department of Civil and Environmental Engineering, University of California, Los Angeles, P.O. Box 159310, Los Angeles, CA 90095-1593, USA
[c] US Army Engineer Research and Development Center, Vicksburg, Mississippi, USA

ARTICLE INFO

Article history:
Received 2 July 2010
Received in revised form 17 January 2011
Available online xxxx

Keywords:
Multi-scale
Damage model
Micro-crack
Homogenization
Helmholtz free energy

ABSTRACT

A class of micro-cracks informed damage models for describing the softening behavior of brittle solids is proposed, in which damage evolution is treated as a consequence of micro-crack propagation. The homogenized stress–strain relation in the cracked microscopic cell defines the degradation tensor, which can be obtained by the equivalence between the averaged strain energy of the microscopic cell and the strain energy density of the homogenized material. This energy equivalence relationship serves as an energy bridging vehicle between the damaged continuum and the cracked microstructure. Several damage evolution equations are obtained by this energy bridging method. The size effect of the micro-cracks informed damage law is characterized through the microscopic cell analysis, and the proper scaling of the characterized damage evolution functions to eliminate mesh dependency in the continuum solution is introduced.

1. Introduction

Continuum damage mechanics (CDM) has been an active research area for more than 50 years (Kachanov, 1958; Robotnov, 1968; Lemaitre and Chaboche, 1974; Mazars, 1984; Ju, 1989; Faria et al., 1998). However, CDM is generally phenomenological, where the damage evolution functions are not related to specific microstructural parameters and local defects. Some earlier efforts have been devoted to the micromechanical investigation of cracked solids (Budiansky and O'connell, 1976; Norris, 1985; Hashin, 1988), however the link to CDM is lacking.

Damage evolution based on a multi-scale framework has been investigated in recent years. Lee et al. (1999) combined the standard finite element method (FEM) with asymptotic homogenization in the undamaged domain and the voronoi cell finite element model (VCFEM) in the damaged region. Fish et al. (1999) proposed a nonlocal damage theory based on asymptotic homogenization to account for damage effects in a heterogeneous media. The reliability of this approach, however, depends on reliability of the micro-scale damage models. Dascalu et al. (2008) and Dascalu (2009) defined the damage variable directly by the micro-crack length. Then a series of differential equations was introduced to describe damage evolution in the microscopic cell based on the homogenization theory and the energy controlled crack propagation. By introducing an internal length in the damage evolution equation, the size effect was characterized.

Damage processes in brittle solids are driven by the distribution of micro-cracks and their evolution. Explicit modeling of micro-cracks in brittle solids is computationally infeasible, while classical damage models are phenomenological in nature; missing the link to microscopic properties. Micromechanics based approaches have been introduced (Nemat-Nasser and Hori, 1999) to obtain homogenized material properties of cracked solids. However, they are limited to certain idealized crack configurations and loading conditions. Alternatively, asymptotic expansion offers a rigorous means for relating physical variables defined at different scales (Benssousan et al., 1978; Bakhvalov and Panasenko, 1989; Guedes and Kikuchi, 1990; Fish et al., 1997). However, the key step in an asymptotic type method is solution of the characteristic functions in the microscopic cell, which is typically very time consuming.

The present work aims at constructing damage models based on thermodynamics of "cracked" microscopic cells and the corresponding "damaged" macroscopic continua. Crack evolution in the microscopic cell is first modeled numerically. Then, corresponding damage evolution functions in the continuum are constructed through a Helmholtz free energy relationship between damaged and undamaged homogenized continua. This approach avoids the tedious solution of characteristic functions in the conventional asymptotic type method.

An outline of this paper is as follows. In Section 2, the two-scale model problem is stated and the homogenization procedures are defined. Based on the homogenized stress and strain, the energy relation between micro- and macro-scales is established in Section 3. In Section 4, procedures for constructing damage evolution functions based on the cracked microscopic cell solution for a

* Corresponding author.
E-mail address: jschen@seas.ucla.edu (J.-S. Chen).

0020-7683/$ - see front matter © 2011 Elsevier Ltd. All rights reserved.
doi:10.1016/j.ijsolstr.2011.02.001

Please cite this article in press as: Ren, X., et al. Micro-cracks informed damage models for brittle solids. Int. J. Solids Struct. (2011), doi:10.1016/j.ijsolstr.2011.02.001

scalar damage model, 2-parameter damage model, and fully tensorial damage model are presented. Numerical formulations for the microscopic cell analysis are given in Section 5. In Section 6, the numerical procedures for energy based characterization of the micro-cracks informed damage model in the continuum scale is discussed, and proper scaling of the characterized damage evolution functions to eliminate mesh dependency of the continuum solution is introduced. Concluding remarks are given in Section 7.

2. Model problem and homogenization operators

We start with a two-scale representation of the model problem. A heterogeneous solid with domain Ω and boundary Γ containing a distribution of micro-cracks is considered, as shown in Fig. 1. The solid is subjected to surface traction $\mathbf{t}$ on Γ_t and prescribed displacement $\bar{\mathbf{u}}$ on Γ_u, $\Gamma_t \cup \Gamma_u = \Gamma$, and is assumed to undergo static elastic deformation without body force. For a given material point in the macroscopic solid, it corresponds to a microscopic cell microstructure with domain Ω_y containing micro-cracks with surface, Γ_c. We use $\mathbf{x}$ as the macroscopic coordinate and $\mathbf{y}$ as the microscopic coordinate.

The boundary-value problem is given as follows:

$$\nabla \cdot \boldsymbol{\sigma}^\varepsilon = 0 \quad \text{in } \Omega \tag{1}$$

with the corresponding boundary conditions,

$$\boldsymbol{\sigma}^\varepsilon \cdot \mathbf{n} = \mathbf{t} \quad \text{on } \Gamma_t \tag{2}$$

$$\mathbf{u}^\varepsilon = \bar{\mathbf{u}} \quad \text{on } \Gamma_u \tag{3}$$

and the effective traction acting on the crack surface,

$$\boldsymbol{\sigma}^\varepsilon \cdot \mathbf{n} = \mathbf{h} \quad \text{on } \Gamma_c \tag{4}$$

where $\boldsymbol{\sigma}^\varepsilon$ is the total stress field, $\mathbf{u}^\varepsilon$ is the total displacement field, superscript "ε" denotes that the coarse and fine scale responses are embedded in the total solution, $\mathbf{n}$ is the unit outward normal vector on the boundary, and the traction $\mathbf{h}$ is applied to the union of crack surfaces Γ_c.

We consider a linear elastic material law:

$$\boldsymbol{\sigma}^\varepsilon = \mathbf{C}^\varepsilon : \mathbf{e}^\varepsilon \tag{5}$$

where $\mathbf{C}^\varepsilon$ is the heterogeneous constitutive tensor, and $\mathbf{e}^\varepsilon$ is the total strain field,

$$\mathbf{e}^\varepsilon = \tfrac{1}{2}(\nabla \otimes \mathbf{u}^\varepsilon + \mathbf{u}^\varepsilon \otimes \nabla) \tag{6}$$

Direct simulation of the total scale governing Eqs. (1)–(4) is time consuming due to the fine-scale microscopic defects and heterogeneities, and an attempt is made to conduct homogenization as shown in Fig. 2, where the homogenized stress and strain are defined by the microscopic cell.

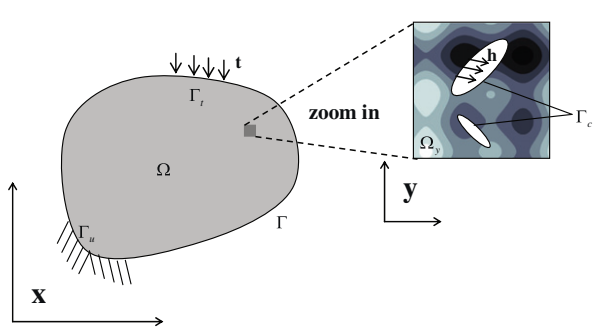

Fig. 1. Microscopic and macroscopic structures.

The tractions and displacements prescribed on the outer boundary of the microscopic cell $\partial\Omega_y$ are related to the homogenized stress and strain in the continuum as:

$$\bar{\boldsymbol{\sigma}} = \frac{1}{V_y} \oint_{\partial\Omega_y} (\mathbf{t}^\varepsilon \otimes \mathbf{x})\, \mathrm{d}s \tag{7}$$

$$\bar{\mathbf{e}} = \frac{1}{2V_y} \oint_{\partial\Omega_y} (\mathbf{u}^\varepsilon \otimes \mathbf{n} + \mathbf{n} \otimes \mathbf{u}^\varepsilon)\, \mathrm{d}s \tag{8}$$

where $V_y = \int_{\Omega_y} \mathrm{d}\Omega$ is the volume of the microscopic cell. Alternatively, the averaged stress and strain in the microscopic cell are defined as

$$\langle \boldsymbol{\sigma}^\varepsilon \rangle = \frac{1}{V_y} \int_{\Omega_y} \boldsymbol{\sigma}^\varepsilon\, \mathrm{d}\Omega \tag{9}$$

$$\langle \mathbf{e}^\varepsilon \rangle = \frac{1}{V_y} \int_{\Omega_y} \mathbf{e}^\varepsilon\, \mathrm{d}\Omega \tag{10}$$

where

$$\langle \cdot \rangle = \frac{1}{V_y} \int_{\Omega_y} \cdot\, \mathrm{d}\Omega \tag{11}$$

The following equation is used to obtain the relation between homogenized and averaged stresses for the cracked microscopic cell:

$$\nabla \cdot (\boldsymbol{\sigma}^\varepsilon \otimes \mathbf{x}) = \nabla \cdot \boldsymbol{\sigma}^\varepsilon \otimes \mathbf{x} + \boldsymbol{\sigma}^\varepsilon \cdot (\nabla \otimes \mathbf{x}) = \boldsymbol{\sigma}^\varepsilon \tag{12}$$

By substituting Eq. (12) into the averaged stress definition in Eq. (9), we have

$$\begin{aligned} \langle \boldsymbol{\sigma}^\varepsilon \rangle &= \frac{1}{V_y} \int_{\Omega_y} \boldsymbol{\sigma}^\varepsilon\, \mathrm{d}\Omega = \frac{1}{V_y} \int_{\Omega_y} \nabla \cdot (\boldsymbol{\sigma}^\varepsilon \otimes \mathbf{x})\, \mathrm{d}\Omega \\ &= \frac{1}{V_y} \oint_{\partial\Omega_y} (\mathbf{t}^\varepsilon \otimes \mathbf{x})\, \mathrm{d}s - \frac{1}{V_y} \oint_{\Gamma_c} (\mathbf{t}^\varepsilon \otimes \mathbf{x})\, \mathrm{d}s \\ &= \bar{\boldsymbol{\sigma}} - \frac{1}{V_y} \oint_{\Gamma_c} (\mathbf{t}^\varepsilon \otimes \mathbf{x})\, \mathrm{d}s \end{aligned} \tag{13}$$

The second term on the right hand side of Eq. (13) vanishes due to equilibrium of the cohesive stresses on the crack surface. Hence the homogenized stress equals to the averaged stress even in the case of a cracked microscopic cell, that is,

$$\bar{\boldsymbol{\sigma}} = \langle \boldsymbol{\sigma}^\varepsilon \rangle \tag{14}$$

Substituting Eq. (6) into averaged strain defined in Eq. (10) and considering the divergence theorem, we have

$$\begin{aligned} \langle \mathbf{e}^\varepsilon \rangle &= \frac{1}{V_y} \int_{\Omega_y} \mathbf{e}^\varepsilon\, \mathrm{d}\Omega = \frac{1}{2V_y} \int_{\Omega_y} (\nabla \otimes \mathbf{u}^\varepsilon + \mathbf{u}^\varepsilon \otimes \nabla)\, \mathrm{d}\Omega \\ &= \frac{1}{2V_y} \oint_{\partial\Omega_y} (\mathbf{u}^\varepsilon \otimes \mathbf{n} + \mathbf{n} \otimes \mathbf{u}^\varepsilon)\, \mathrm{d}s - \frac{1}{2V_y} \\ &\quad \times \oint_{\Gamma_c} (\mathbf{u}^\varepsilon \otimes \mathbf{n} + \mathbf{n} \otimes \mathbf{u}^\varepsilon)\, \mathrm{d}s \\ &= \bar{\mathbf{e}} - \frac{1}{2V_y} \oint_{\Gamma_c} (\mathbf{u}^\varepsilon \otimes \mathbf{n} + \mathbf{n} \otimes \mathbf{u}^\varepsilon)\, \mathrm{d}s \end{aligned} \tag{15}$$

Consequently we obtain the relation between homogenized strain and averaged strain as follows

$$\bar{\mathbf{e}} = \langle \mathbf{e}^\varepsilon \rangle + \frac{1}{2V_y} \oint_{\Gamma_c} (\mathbf{u}^\varepsilon \otimes \mathbf{n} + \mathbf{n} \otimes \mathbf{u}^\varepsilon)\, \mathrm{d}s \tag{16}$$

Here it is shown that the homogenized strain consists of the average strain and the additional strain induced by the displacement jump across the crack surfaces. In other words, macroscopic strain cannot be directly obtained by the averaging of microscopic strain when micro-cracks exist.

Please cite this article in press as: Ren, X., et al. Micro-cracks informed damage models for brittle solids. Int. J. Solids Struct. (2011), doi:10.1016/j.ijsolstr.2011.02.001

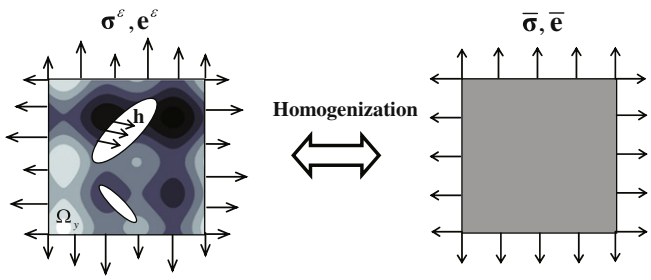

Fig. 2. Homogenization of microscopic cell with fluctuating fields.

To obtain the homogenized material tensor, we define the fourth order influence tensor as:

$$\mathbf{e}^{\varepsilon}(\mathbf{x}) = \left[\mathbf{I} - \mathbf{A}^{\varepsilon}(\mathbf{x})\right] : \bar{\mathbf{e}} \tag{17}$$

where $\mathbf{I}$ is the fourth order identity tensor. Substituting Eq. (17) into the stress–strain relation in Eq. (5), we have

$$\boldsymbol{\sigma}^{\varepsilon} = \mathbf{C}^{\varepsilon} : \mathbf{e}^{\varepsilon} = \mathbf{C}^{\varepsilon} : \left[\mathbf{I} - \mathbf{A}^{\varepsilon}(\mathbf{x})\right] : \bar{\mathbf{e}} \tag{18}$$

Using the equivalence between the homogenized stress and averaged stress, we obtain

$$\bar{\boldsymbol{\sigma}} = \langle \mathbf{C}^{\varepsilon} : [\mathbf{I} - \mathbf{A}^{\varepsilon}(\mathbf{x})] \rangle : \bar{\mathbf{e}} \equiv \bar{\mathbf{C}} : \bar{\mathbf{e}} \tag{19}$$

From the above equation, we express the homogenized material response tensor as

$$\bar{\mathbf{C}} = (\mathbf{I} - \mathbf{D}) : \langle \mathbf{C}^{\varepsilon} \rangle \tag{20}$$

where

$$\mathbf{D} = \langle \mathbf{C}^{\varepsilon} : \mathbf{A}^{\varepsilon} \rangle : \langle \mathbf{C}^{\varepsilon} \rangle^{-1} \tag{21}$$

Here $\mathbf{D}$ is a degradation (damage) tensor expressed by the influence tensor $\mathbf{A}^{\varepsilon}(\mathbf{x})$.

Remark 2.1. The fourth order influence tensor $\mathbf{A}^{\varepsilon}(\mathbf{x})$ represents the inter-scale relation between properties of the cracked microstructures and properties of the homogenized continua. Micromechanics offers an analytical bases for obtaining the influence tensor, for example, Mori–Tanaka method (Mori and Tanaka, 1973), self-consistent method (Budiansky and O'connell, 1976) and differential scheme (Norris, 1985). On the other hand, asymptotic expansion based homogenization offers a general approach for calculating the influence tensor, which utilizes the numerical solution of characteristic functions for scale-coupling in the microscopic cell.

Remark 2.2. Using the asymptotic expansion based method, the influence tensor can be obtained from the characteristic tensor $\boldsymbol{\chi}(\mathbf{y})$ (detailed derivations see Appendix A):

$$\mathbf{A}^{\varepsilon} = -\nabla^{s}_{\mathbf{y}} \boldsymbol{\chi}(\mathbf{y}) \tag{22}$$

where the characteristic tensor $\boldsymbol{\chi}(\mathbf{y})$ is solved from the following boundary-value problem defined in the microscopic cell:

$$\nabla_{\mathbf{y}} \cdot \left(\mathbf{C}^{\varepsilon} : \nabla^{s}_{\mathbf{y}} \boldsymbol{\chi}(\mathbf{y})\right) = 0 \quad \text{in } \Omega_y \tag{23}$$

$$\left[\mathbf{C}^{\varepsilon} : \nabla^{s}_{\mathbf{y}} \boldsymbol{\chi}(\mathbf{y}) : \nabla^{s}_{\mathbf{x}} \mathbf{v}^{[0]}(\mathbf{x})\right] \cdot \mathbf{n} = -\left[\mathbf{C}^{\varepsilon} : \nabla^{s}_{\mathbf{x}} \mathbf{v}^{[0]}(\mathbf{x})\right] \cdot \mathbf{n} + \mathbf{h} \quad \text{on } \Gamma_c \tag{24}$$

Clearly the numerical solution of the above boundary-value problem for obtaining the third order tensor $\boldsymbol{\chi}(\mathbf{y})$ is computationally intensive. This issue is addressed by introducing the energy bridging method as discussed in the next section.

3. Energy bridging between scales

To establish the relationship between the micro-cracks induced material degradation and the damaged continuum described by conventional damage mechanics, the Helmholtz free energy (HFE) is employed:

$$\overline{\Psi} = \tfrac{1}{2} \bar{\boldsymbol{\sigma}} : \bar{\boldsymbol{e}} \tag{25}$$

According to the second principle of thermodynamics, we have

$$\bar{\boldsymbol{\sigma}} = \frac{\partial \overline{\Psi}}{\partial \bar{\mathbf{e}}} \tag{26}$$

$$\mathbf{Y} = -\frac{\partial \overline{\Psi}}{\partial \mathbf{D}} \tag{27}$$

where $\mathbf{D}$ is the damage tensor and $\mathbf{Y}$ is the damage energy release rate (DERR) representing a driving force of damage evolution. Consequently, the damage evolution equation is expressed by the evolution potential, Φ, as follows

$$\dot{\mathbf{D}} = \dot{\lambda} \frac{\partial \Phi}{\partial \mathbf{Y}} \tag{28}$$

where λ is the consistency parameter. In conventional continuum damage mechanics, HFE is determined experientially. In the present approach, the HFE is obtained through homogenization of the cracked microstructure. The microscopic free energy is defined as

$$\Psi^{\varepsilon} = \tfrac{1}{2} \boldsymbol{\sigma}^{\varepsilon} : \mathbf{e}^{\varepsilon} \tag{29}$$

where $\boldsymbol{\sigma}^{\varepsilon}$and $\mathbf{e}^{\varepsilon}$ are the microscopic stress and strain. Integrating microscopic HFE in the microscopic cell yields

$$\begin{aligned} \int_{\Omega_y} \Psi^{\varepsilon} \, \mathrm{d}\Omega &= \frac{1}{2} \int_{\Omega_y} \boldsymbol{\sigma}^{\varepsilon} : \mathbf{e}^{\varepsilon} \, \mathrm{d}\Omega = \frac{1}{2} \int_{\Omega_y} \frac{1}{2} \boldsymbol{\sigma}^{\varepsilon} : (\nabla \otimes \mathbf{u}^{\varepsilon} + \mathbf{u}^{\varepsilon} \otimes \nabla) \, \mathrm{d}\Omega \\ &= \frac{1}{2} \int_{\Omega_y} \frac{1}{2} [\nabla \cdot (\mathbf{u}^{\varepsilon} \cdot \boldsymbol{\sigma}^{\varepsilon}) + \nabla \cdot (\boldsymbol{\sigma}^{\varepsilon} \cdot \mathbf{u}^{\varepsilon}) - \mathbf{u}^{\varepsilon} \cdot \nabla \cdot \boldsymbol{\sigma}^{\varepsilon} \\ &\quad - \nabla \cdot \boldsymbol{\sigma}^{\varepsilon} \cdot \mathbf{u}^{\varepsilon}] \, \mathrm{d}\Omega = \frac{1}{2} \int_{\Omega_y} \nabla \cdot (\mathbf{u}^{\varepsilon} \cdot \boldsymbol{\sigma}^{\varepsilon}) \, \mathrm{d}\Omega \end{aligned} \tag{30}$$

Note that we have used equilibrium without body force. Introducing the divergence theorem in Eq. (30) results in

$$\begin{aligned} \int_{\Omega_y} \Psi^{\varepsilon} \, \mathrm{d}\Omega &= \frac{1}{2} \int_{\Omega_y} \nabla \cdot (\mathbf{u}^{\varepsilon} \cdot \boldsymbol{\sigma}^{\varepsilon}) \, \mathrm{d}\Omega \\ &= \frac{1}{2} \oint_{\partial\Omega_y} \mathbf{u}^{\varepsilon} \cdot \boldsymbol{\sigma}^{\varepsilon} \cdot \mathbf{n} \, \mathrm{d}s - \frac{1}{2} \oint_{\Gamma_c} \mathbf{u}^{\varepsilon} \cdot \boldsymbol{\sigma}^{\varepsilon} \cdot \mathbf{n} \, \mathrm{d}s \\ &= \frac{1}{2} \oint_{\partial\Omega_y} \mathbf{u}^{\varepsilon} \cdot \mathbf{t}^{\varepsilon} \, \mathrm{d}s - \frac{1}{2} \oint_{\Gamma_c} \mathbf{u}^{\varepsilon} \cdot \mathbf{h} \, \mathrm{d}s \end{aligned} \tag{31}$$

Here we consider a strain driven homogenization, where the displacement boundary conditions obtained from macroscopic strain are applied to the microscopic cell to compute the local stress field. The local stress field is then averaged, which is the same as the homogenized stress $\bar{\boldsymbol{\sigma}}$ according to Eq. (14), and is passed back to the coarse scale. The prescribed boundary displacements on the microscopic cell are obtained from the macroscopic strain by

$$\mathbf{u}^{\varepsilon} = \bar{\mathbf{e}} \cdot \mathbf{x} \quad \text{on } \partial\Omega_y \tag{32}$$

where $\partial\Omega_y$ is the outer boundary of the microscopic cell. Substituting Eq. (32) into the first term on the right hand side of Eq. (31), we have

$$\begin{aligned} \frac{1}{2} \oint_{\partial\Omega_y} \mathbf{u}^{\varepsilon} \cdot \mathbf{t}^{\varepsilon} \, \mathrm{d}s &= \frac{1}{2} \oint_{\partial\Omega_y} (\bar{\mathbf{e}} \cdot \mathbf{x}) \cdot \mathbf{t}^{\varepsilon} \, \mathrm{d}s = \frac{1}{2} \left[\oint_{\partial\Omega_y} (\mathbf{t}^{\varepsilon} \otimes \mathbf{x}) \, \mathrm{d}s \right] : \bar{\mathbf{e}} \\ &= \frac{V_y}{2} \bar{\boldsymbol{\sigma}} : \bar{\mathbf{e}} = V_y \overline{\Psi} \end{aligned} \tag{33}$$

Combining Eqs. (31) and (33) we have

$$\overline{\Psi} = \frac{1}{V_y} \left(\int_{\Omega_y} \Psi^{\varepsilon} \, \mathrm{d}\Omega + \frac{1}{2} \oint_{\Gamma_c} \mathbf{u}^{\varepsilon} \cdot \mathbf{h} \, \mathrm{d}s \right) \tag{34}$$

The right hand side of (34) is the averaged free energy of the microscopic cell, while the left hand side of (34) is the energy density of the homogenized material. Thus Eq. (34) concludes that the averaged energy of the microscopic cell is equal to the energy density of the homogenized material.

Remark 3.1. The result in Eq. (34) is an extension of Hill's theorem (Hill, 1963), with addition of the second term on the right hand side resulting from the crack discontinuous displacement field. This result is consistent with the one obtained by Belytschko et al. (2008) where the power expression of the energy bridging equation has been introduced. Further, the energy equivalence in Eq. (34) can also be obtained by the asymptotic expansion approach as detailed in Appendix B.

4. Characterization of parameters in continuum damage mechanics by energy bridging

We use the Helmholtz free energy relationship between the homogenized continuum and the cracked microstructure to derive damage parameters for several commonly used damage models.

4.1. One-parameter scalar damage model

The one-parameter damage model (Mazars, 1984) is expressed as

$$\overline{\Psi} = (1-d)\Psi_0 \tag{35}$$

where $\overline{\Psi}$ is Helmholtz free energy computed from the microscopic cell in Eq. (34), and Ψ_0 is the effective Helmholtz free energy obtained by

$$\Psi_0 = \tfrac{1}{2}\bar{\mathbf{e}} : \overline{\mathbf{C}}_0 : \bar{\mathbf{e}} \tag{36}$$

where $\overline{\mathbf{C}}_0$ is the homogenized undamaged material tensor. Then the damage scalar is obtained by

$$d = 1 - \frac{\overline{\Psi}}{\Psi_0} \tag{37}$$

4.2. Two-parameter damage model

The two-parameter damage model has been extensively studied and widely adopted for description of more complicated damage mechanisms (Faria et al., 1998; Wu et al., 2006; Li and Ren, 2009). For geological materials such as sand or soil, the volumetric–deviatoric splitting approach has been adopted to describe damage mechanisms driven by pressure and shear. On the other hand, the hydrostatic tension–compression decomposition approach has been used for quasi-brittle materials like concrete and rock (Faria et al., 1998), which is the case demonstrated herein. The framework of the two-parameter damage model is described in Appendix C.

The initially undamaged macroscopic stress is obtained as

$$\bar{\boldsymbol{\sigma}}_0 = \overline{\mathbf{C}}_{\mathbf{0}} : \bar{\mathbf{e}} \tag{38}$$

The macroscopic stress can be decomposed as

$$\bar{\boldsymbol{\sigma}}_0 = \bar{\boldsymbol{\sigma}}_0^+ + \bar{\boldsymbol{\sigma}}_0^- \tag{39}$$

where $\bar{\boldsymbol{\sigma}}_0^+$ and $\bar{\boldsymbol{\sigma}}_0^-$ are the tensile and compressive stresses, respectively, defined as

$$\bar{\boldsymbol{\sigma}}_0^+ = \sum_i \hat{\sigma}_i H(\hat{\sigma}_i)\mathbf{p}_i \otimes \mathbf{p}_i \tag{40}$$

$$\bar{\boldsymbol{\sigma}}_0^- = \bar{\boldsymbol{\sigma}}_0 - \bar{\boldsymbol{\sigma}}_0^+ \tag{41}$$

$\hat{\sigma}_i$ and $\mathbf{p}_i$ are the ith eigenvalue and the corresponding eigenvector of $\bar{\boldsymbol{\sigma}}_0$, and $H(\cdot)$ is the Heaviside function.

The macroscopic Helmholtz free energy is then expressed as

$$\overline{\Psi} = (1-d^+)\Psi_0^+ + (1-d^-)\Psi_0^- \tag{42}$$

where d^+ and d^- are tensile and compressive damage parameters, respectively, and the corresponding expressions of the effective Helmholtz free energy are

$$\Psi_0^\pm = \tfrac{1}{2}\bar{\boldsymbol{\sigma}}_0^\pm : \overline{\mathbf{C}}_0^{-1} : \bar{\boldsymbol{\sigma}}_0^\pm \tag{43}$$

Consider the Clausius–Duhem inequality of irreversible thermodynamics, the following can be derived from the Helmholtz free energy in Eq. (42):

$$Y^\pm = \Psi_0^\pm \tag{44}$$

and

$$d^\pm = 1 - \frac{\partial\overline{\Psi}}{\partial Y^\pm} \approx 1 - \frac{\Delta\overline{\Psi}}{\Delta Y^\pm} \tag{45}$$

where $\overline{\Psi}$ is the Helmholtz free energy calculated from the microscopic cell in Eq. (34). By using the finite difference operation in Eq. (45), the evolution of damage parameters is obtained.

4.3. Fully tensorial damage model

Derivation of the tensorial damage tensor based on the influence tensor $\mathbf{A}^\varepsilon(\mathbf{x})$ according to Eq. (21) is limited to special cases if $\mathbf{A}^\varepsilon(\mathbf{x})$ is obtained by micromechanical methods, and is costly if $\mathbf{A}^\varepsilon(\mathbf{x})$ is calculated using the asymptotic expansion method. By introducing bridging based on Helmholtz free energy, a more efficient approach for obtaining the damage tensor is introduced. Recall the definition of the macroscopic Helmholtz free energy in Eq. (25), we have

$$\overline{\Psi} = \tfrac{1}{2}\bar{\mathbf{e}} : (\mathbf{I} - \mathbf{D}) : \overline{\mathbf{C}}_{\mathbf{0}} : \bar{\mathbf{e}} \tag{46}$$

Performing partial differentiation of the Helmholtz free energy in Eq. (46) with respect to the fourth order damage tensor, $\mathbf{D}$, we obtain the damage energy release rate as follows

$$\mathbf{Y} = -\frac{\partial\overline{\Psi}}{\partial\mathbf{D}} = \frac{1}{2}\bar{\mathbf{e}} : \overline{\mathbf{C}}_{\mathbf{0}} : \bar{\mathbf{e}} \tag{47}$$

By taking the derivative of the Helmholtz free energy of the microscopic cell in Eq. (34) with respect to the damage energy release rate, $\mathbf{Y}$, we obtain the fourth order damage tensor:

$$\mathbf{D} = \boldsymbol{I} - \frac{\partial\bar{\Psi}}{\partial\mathbf{Y}} \approx \boldsymbol{I} - \frac{\Delta\overline{\Psi}}{\Delta\mathbf{Y}} \tag{48}$$

Here a finite difference approach could be used in Eq. (48) to obtain the fourth order damage tensor using$\Delta\overline{\Psi}$ and $\Delta\mathbf{Y}$.

5. Microscopic cell analysis

The essential step in obtaining the damage evolution functions in the proposed method is the microscopic cell analysis. In the present study, the microscopic cell is made of an isotropic linear elastic material with a center crack subjected to boundary conditions as shown in Fig. 3. The boundary conditions on the microscopic cell are defined based on the type of damage mechanisms to be captured. The crack is modeled by a cohesive crack model with linear degradation as shown in Fig. 3. The crack propagation direction is determined by the maximum hoop stress criterion.

In this work, we consider an enriched reproducing kernel particle method (RKPM) for the microscopic cell analysis. The microscopic cell solution is then used in the homogenization as

described in Section 4 for characterization of the damage parameter evolution.

In RKPM (Liu et al., 1995; Chen et al., 1996), the approximation of a function u is expressed as

$$u^h(\mathbf{x}) = \sum_I \phi_I(\mathbf{x}) u_I \tag{49}$$

where $\phi_I(\mathbf{x})$ is the reproducing kernel (RK) shape function and u_I is the corresponding coefficient. In the following, we use multi-dimensional notation: $\alpha = (\alpha_1, \alpha_2, \ldots, \alpha_d)$, $|\alpha| = \sum_{i=1}^{d} \alpha_i$, $\boldsymbol{x}^\alpha = x_1^{\alpha_1} \cdots x_d^{\alpha_d}$, $\boldsymbol{x}_I^\alpha = x_{1I}^{\alpha_1} \cdots x_{dI}^{\alpha_d}$, and d is the spatial dimension. The RK shape functions are constructed using monomials as basis functions expressed as

$$\phi_I(\boldsymbol{x}) = \varphi_a(\mathbf{x} - \mathbf{x}_I) \left(\sum_{|\alpha| \leqslant n} (\mathbf{x} - \mathbf{x}_I)^\alpha b_\alpha(\mathbf{x}) \right) \tag{50}$$

where $\varphi_a(\mathbf{x} - \mathbf{x}_I)$ is the kernel function with support size a, $\{(\mathbf{x} - \mathbf{x}_I)^\alpha\}_{|\alpha| \leqslant n}$ is the set of monomial basis functions, and $\{b_\alpha(\mathbf{x})\}_{|\alpha| \leqslant n}$ are the coefficients of the basis functions obtained by imposing the following reproducing conditions:

$$\sum_I \phi_I(\mathbf{x}) \mathbf{x}_I^\alpha = \mathbf{x}^\alpha, \quad |\alpha| \leqslant n \tag{51}$$

Obtaining $b_\alpha(\mathbf{x})$ from (51), the RK shape function is constructed:

$$\phi_I(\mathbf{x}) = \mathbf{H}^T(\mathbf{0}) \mathbf{M}^{-1}(\mathbf{x}) \mathbf{H}^T(\mathbf{x} - \mathbf{x}_I) \varphi_a(\boldsymbol{x} - \boldsymbol{x}_I) \tag{52}$$

where $\mathbf{H}(\mathbf{x}) = \{\mathbf{x}^\alpha\}_{|\alpha| \leqslant n} = \{1, x_1, \ldots, x_d^n\}$ is the vector containing all the basis functions and $\mathbf{M}$ is the moment matrix defined as

$$\mathbf{M}(\mathbf{x}) = \sum_I \mathbf{H}(\mathbf{x} - \mathbf{x}_I) \mathbf{H}^T(\mathbf{x} - \mathbf{x}_I) \varphi_a(\boldsymbol{x} - \boldsymbol{x}_I) \tag{53}$$

To consider enrichment of RKPM by a set of enrichment functions, $p_i(\mathbf{x})$, the following reproducing conditions are introduced (Fleming et al., 1997):

$$Q_i(\mathbf{x}) = \sum_I \phi_I(\mathbf{x}) Q_i(\mathbf{x}_I) + p_i(\mathbf{x}) \tag{54}$$

where $Q_i(\mathbf{x})$ is the target function and $p_i(\mathbf{x})$is the corresponding enrichment. The enrichment is thus expressed as

$$p_i(\mathbf{x}) = Q_i(\mathbf{x}) - \sum_I \phi_I(\mathbf{x}) Q_i(\mathbf{x}_I) \tag{55}$$

The enriched RKPM is given in the following form:

$$u^h(\mathbf{x}) = \sum_I \phi_I(\mathbf{x}) u_I + \sum_i k_i \left\{ Q_i(\mathbf{x}) - \sum_I \phi_I(\mathbf{x}) Q_i(\mathbf{x}_I) \right\} \tag{56}$$

where k_i is the coefficient of the enrichment function p_i. For the microscopic cell analysis, the following target functions for enrichment of the crack tip solution (Möes and Belytschko, 2002) have been introduced:

$$\begin{cases} [Q_1, Q_2, Q_3, Q_4] = \left[\sqrt{r}\sin\left(\frac{\theta}{2}\right), \sqrt{r}\cos\left(\frac{\theta}{2}\right), \sqrt{r}\sin\left(\frac{\theta}{2}\right)\sin\theta, \right. \\ \qquad \left. \sqrt{r}\cos\left(\frac{\theta}{2}\right)\sin\theta\right] \quad \text{for LEFM} \\ [Q_1, Q_2, Q_3] = \left[r\sin\left(\frac{\theta}{2}\right), r^{\frac{3}{2}}\sin\left(\frac{\theta}{2}\right), r^2\sin\left(\frac{\theta}{2}\right)\right] \\ \qquad \text{for Cohesive Crack Model} \end{cases} \tag{57}$$

The functional for the microscopic cell problem is expressed as

$$\Pi = \frac{1}{2} \int_{\Omega_y} \varepsilon_{ij} C_{ijkl} \varepsilon_{kl} \, \mathrm{d}\Omega - \int_{\Gamma_t} u_i \bar{t}_i \, \mathrm{d}\Gamma + \frac{\alpha}{2} \int_{\Gamma_u} (u_i - \bar{u}_i)(u_i - \bar{u}_i) \, \mathrm{d}\Gamma \tag{58}$$

where α is the penalty parameter for imposing the essential boundary conditions. Introducing the enriched RK approximation in Eq. (56) into the stationary condition of Eq. (58), we have

$$(\mathbf{K} + \alpha \mathbf{K}_u)\mathbf{U} = \mathbf{f} + \alpha \mathbf{f}_u \tag{59}$$

where $\mathbf{K}$ is the stiffness matrix, $\mathbf{f}$ is the force vector, and $\mathbf{K}_u$ and $\mathbf{f}_u$ are the terms associated with imposition of essential boundary conditions. For the simulation of solids, the penalty parameter α is chosen to be 10^3–$10^6 E$ where E is the elastic modulus.

6. Numerical tests

In the aforementioned homogenization calculation of damage parameters, modeling of the microscopic cell with micro-cracks propagation as described in Section 5 is first performed. The microscopic cell analysis results are then processed according to the homogenization procedures in Sections 3 and 4 to obtain the evolution of damage parameters. It is noted that the homogenized damage evolution functions need to be properly scaled with respect to the ratio between dimensions of the microscopic cell and mesh to avoid the "numerical size effect". This will be discussed in the following section.

A notched beam under three point bending, as shown in Fig. 4, is to be modeled by the proposed methods. This problem has been extensively studied both experimentally (Petersson, 1981) and numerically (de Borst, 1986 and Meyer et al., 1994). The overall behavior of the beam is governed by the Mode I crack initiated at the vertex of the notch. Hence the microscopic cell model with an evolving Mode I crack is considered for generation of the damage evolution function. In this example, we consider the two-parameter damage model as given in Section 4.2 with the compressive damage evolution suppressed due to the bending condition and moderate beam thickness. The material properties of elastic modulus and Poisson's ratio are 30 GPa and 0.2, respectively. Tensile strength of the material is f_u = 3.33 MPa, and fracture energy of the cohesive crack is G_I = 124 N/m (de Borst, 1986).

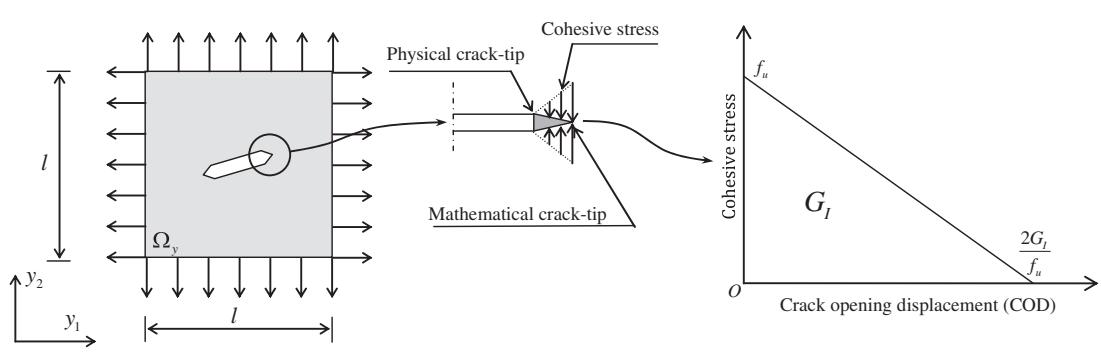

Fig. 3. Microscopic cell problem and cohesive crack model.

Please cite this article in press as: Ren, X., et al. Micro-cracks informed damage models for brittle solids. Int. J. Solids Struct. (2011), doi:10.1016/j.ijsolstr.2011.02.001

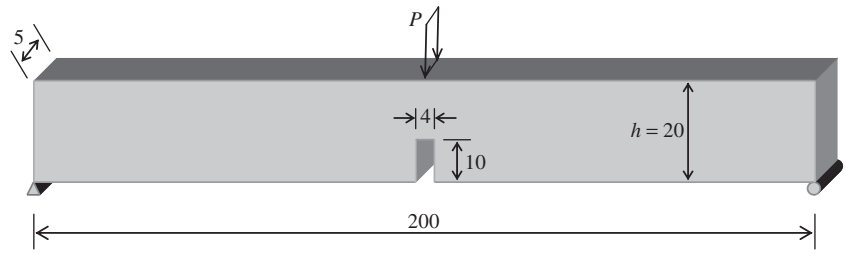

Fig. 4. Notched beam subjected to three-point bending (unit: cm).

6.1. Characterization of damage evolution functions

The microscopic cell geometry with initial crack and boundary conditions are shown in Fig. 3. We consider a microscopic cell subjected to uniform tension with a centered crack propagating perpendicular to the loading direction. In this study, the initial crack length is set to be one-tenth of the microscopic cell dimension. Based on the numerical method described in Section 5, we first obtain the stress and strain fields in the microscopic cell at different loading stages. Normal stresses in the direction of loading at different stages of crack propagation are shown in Fig. 5. The homogenized stress and strain are shown in Fig. 6(a). The energy bridging Eq. (34) is employed to calculate the damage variable as a function of deformation as discussed in Section 5. The homogenized tensile damage evolution is shown in Fig. 6(b).

Here we study the size effect by considering various sizes of microscopic cells which correspond to structural models with coarse, medium and fine meshes. For this purpose, define a dimensionless parameter, λ, as the ratio between the microscopic length parameter l_{mic} and the macroscopic length parameterl_{mac}. Here we consider the dimension of the microscopic cell l and height of the beam h as the two-scale parameters and define their ratio as:

$$\lambda = \frac{l_{mic}}{l_{mac}} = \frac{l}{h} \tag{60}$$

It is observed in Fig. 7 that the homogenized stress–strain curves are strongly affected by the size of the microscopic cell. The cohesive law employed in the microscopic analysis of crack propagation involves a length scale, which is the crack opening displacement corresponding to zero stress ($2G_I/f$ in Fig. 3), called the critical crack opening displacement. This length scale does not scale with the microscopic cell, and thus leads to different homogenized stress–strain curves based on different cell dimensions. As the cell dimension increases, the homogenized strain corresponding to the critical crack opening displacement decreases, and yields strain softening with a larger negative slope as shown in Fig. 7. Computationally, the macroscopic mesh dimension is used to represent the averaged material behavior within the mesh. Thus if the cohesive law is used in a microscopic cell for obtaining the homogenized stress–strain curve for a macroscopic calculation, the corresponding microscopic cell dimension needs to be dimensionally close to the mesh dimension when strain softening exists for the above said reason. Unfortunately this is practically tedious for arbitrary mesh geometry. Therefore, a scaling law will be introduced in the following discussion so that the homogenized stress–strain curves for different mesh points are scaled based on a "reference microscopic cell analysis".

It is also noted that as the microscopic cell size increases, the energy dissipation capacity of the microscopic cell (the area under the stress–strain curve) decreases. The reason is that the energy dissipated by the cohesive crack propagation is dominated by the elastic energy within the microscopic cell as its size increases. For the microscopic cell with dimension exceeding the dimension of the macroscopic solid, its elastic energy becomes greater than the cohesive crack opening energy, hence the snap-back behavior as shown in Fig. 7 for λ = 5,10. Fig. 8(a) demonstrates the size dependence of the calculated nominal strength which can be well fitted to the size effect law proposed by Bazant (1984):

$$\sigma_N = \frac{Bf_u}{\sqrt{1+\beta}}, \qquad \beta = \frac{l}{l_0} \tag{61}$$

where f_u is the tensile strength of concrete, l is the specimen dimension, and B and l_0 are material parameters identified by experimental data or numerical simulation. This size dependent property is due to influence of the internal length scale, i.e., the crack opening displacement characteristic length, which does not scale with the overall dimension of the microscopic cell and specimen. The scale dependence of rupture strain, ε_u, is also shown in Fig. 8(b), where a size effect law for ε_u can also be extracted from numerical results.

For microscopic cells with different dimensions and with the center crack dimension defined in proportion with the microscopic cell dimension, the homogenized damage evolution curves takes different paths from 0 to 1, as can be seen in Fig. 9. Note that a critical size l_c for the microscopic cell exists. This inherent critical size represents the constraint on the discretization of the macroscopic structures.

Remark 6.1. Besides the dimension of the microscopic cell, the characterized macroscopic damage evolution is also affected by the criteria of the micro-crack propagation. While cohesive energy has been employed in this work as the crack propagation criterion, for general applications it should be carefully investigated according to the key characteristics of material behavior.

6.2. Mesh insensitive solution by scaled damage evolution functions

The characterized tensile damage evolution equation for two-parameter damage model, given in Section 6.1, is employed in the structural level analysis based on continuum damage mechanics. Due to softening behavior of the material response, the arc-length method is used for the nonlinear analysis. To study mesh sensitivity of the multi-scale analysis, coarse, medium and fine meshes are constructed for the notched beam as shown in Fig. 10.

In the conventional damage models, the damage evolution curves are directly used in the structural analysis without consideration of the relationship between microstructure dimension and mesh size. Fig. 11 shows a strong mesh dependency induced by this standard procedure where only one microscopic cell is used to characterize the damage evolution equation without use of the scaling law in Eq. (61) and linear fit of Fig. 8(b). With the proposed method, the micro-cracks induced damage evolution curve is first characterized by the cracked microscopic cell simulation results. By introducing the scaled damage evolution curves in Fig. 9 according to the mesh dimension, the mesh independent results are obtained. The agreement between numerical results with different

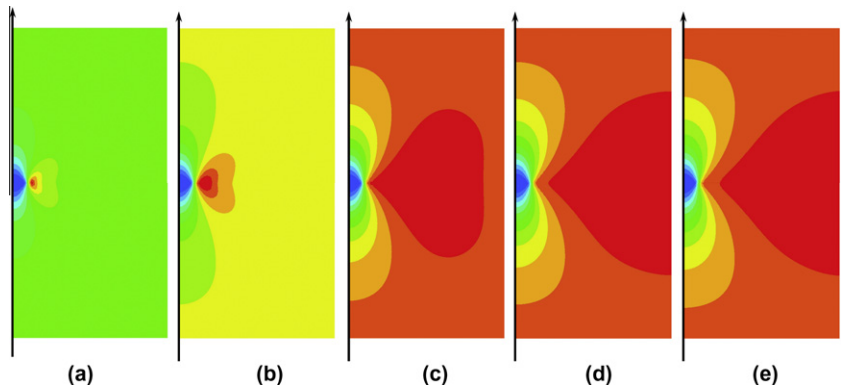

Fig. 5. Normal stress contours (in direction of loading) at different loading stages.

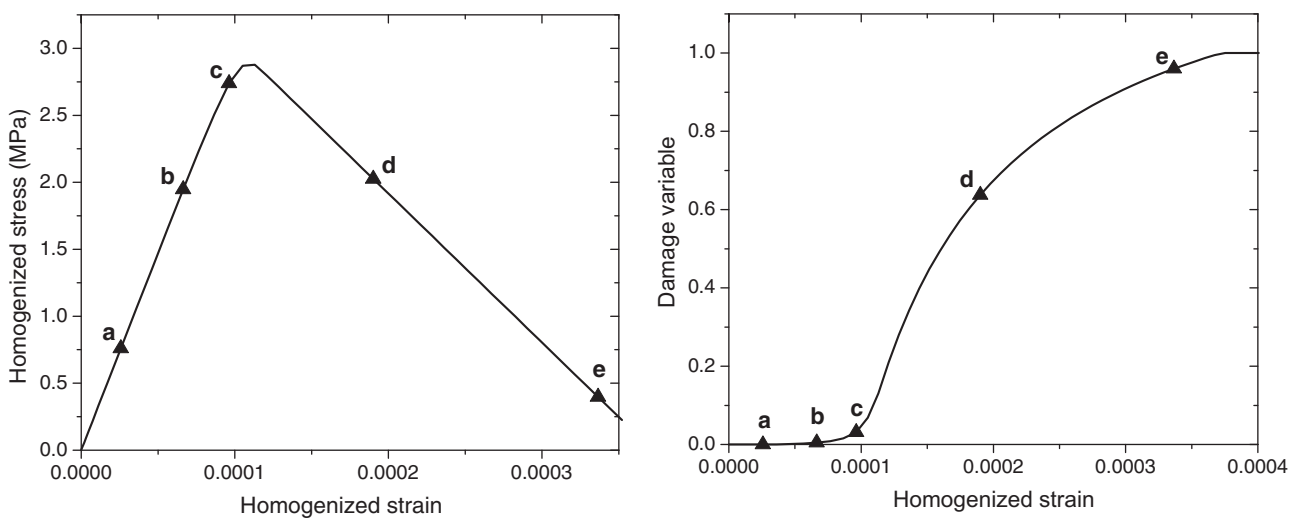

(a) Homogenized stress-strain curve

(b) Homogenized damage evolution

Fig. 6. (a) Homogenized stress and strain and (b) tensile damage parameter calculated by the microscopic stress and strain fields, where a, b, c, d and e denote the corresponding homogenized stresses, strains and damage parameters calculated based on the stress fields (a), (b), (c), (d) and (e) shown in Fig. 5, respectively.

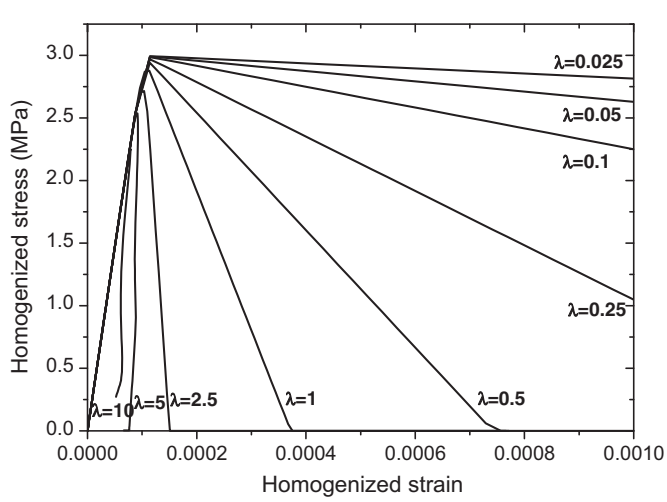

Fig. 7. Homogenized stress–strain curves.

mesh refinements and the benchmark results (from Abaqus 6.5 user's manual (2005)) is shown in Fig. 12. The stress and strain contours representing damage evolution in the structures are shown in Figs. 13 and 14.

Remark 6.2. The macroscopic mesh is a numerical representation of the solids included within its domain, and the stress–strain relation introduced in the quadrature points describes the homogenized behavior of the solid within the mesh. For an elastic solid, the homogenized stress–strain curve is insensitive to the mesh dimension, and thus no mesh dependency issues exist for elastic problem. On the other hand, the softening solid typically involves length scales in the material laws, for example, the ones constructed by homogenization of microscopic fracture analysis with cohesive law introduced in this work. When the length scales in the material laws do not scale properly with the representative domain of the macroscopic quadrature points, mesh dependent results arise. In the present work, the mesh dependency in the softening problem is removed by adopting a scaling law to a "reference homogenized stress–strain curve" obtained from a reference microscopic cell analysis.

7. Conclusions

In this work, we consider damage in the continua as the homogenization of micro-cracks in the microstructures. Bridging between the cracked microstructure and the damaged continuum is facilitated by the equivalence of Helmholtz free energy between the two scales. As such, damage in the continua represented by the

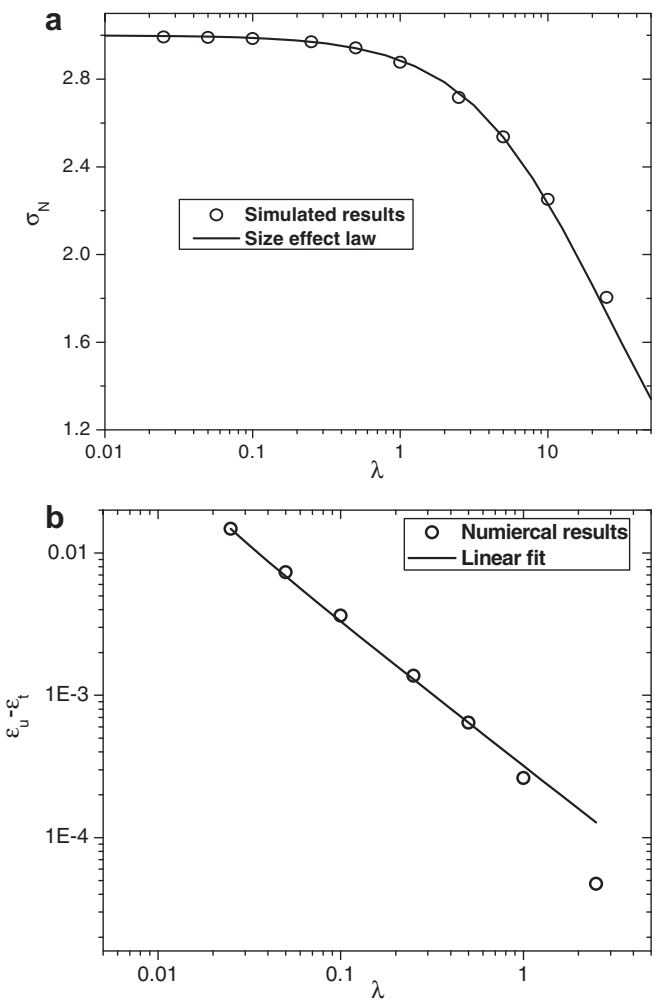

Fig. 8. Size dependent of microscopic cells: (a) nominal strength; (b) difference between rupture strain ε_u and peak strain ε_t.

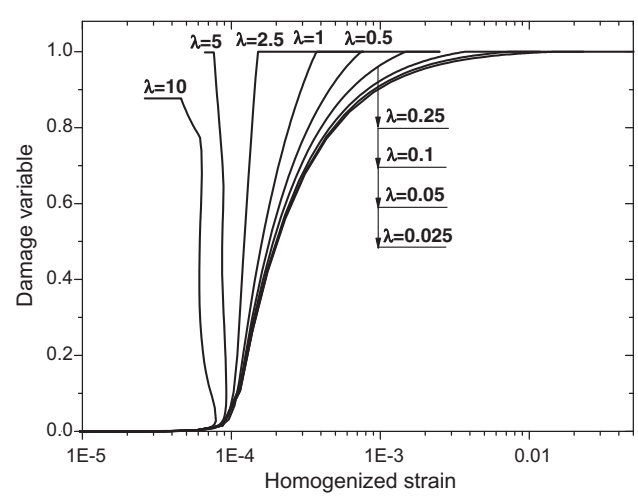

Fig. 9. Micro-cracks informed damage evolutions.

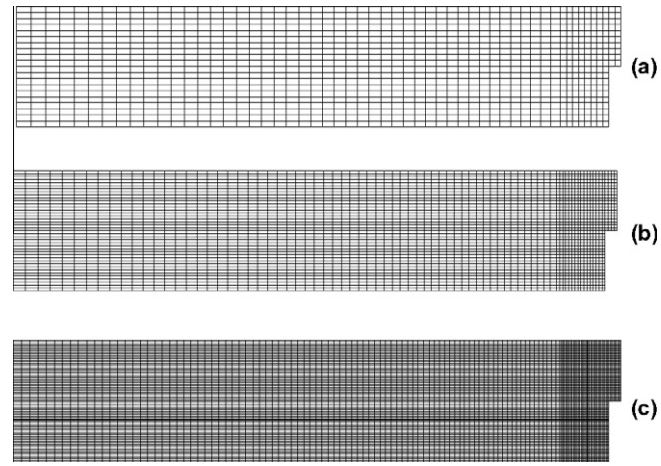

Fig. 10. Finite element mesh with different levels of refinement: (a) coarse mesh, (b) medium mesh and (c) fine mesh.

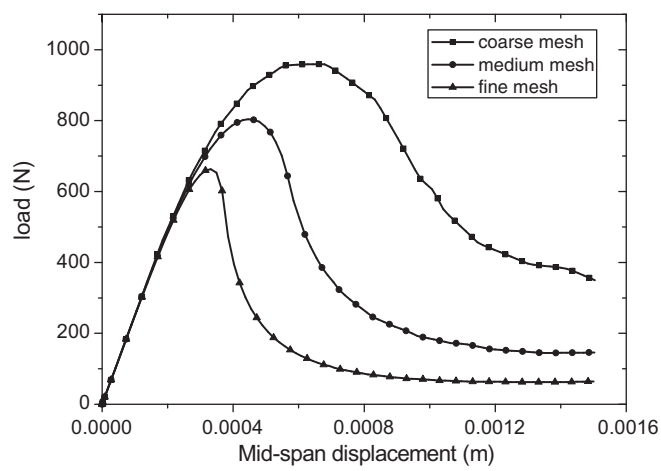

Fig. 11. Mesh dependent load–displacement responses using inconsistent microscopic cell.

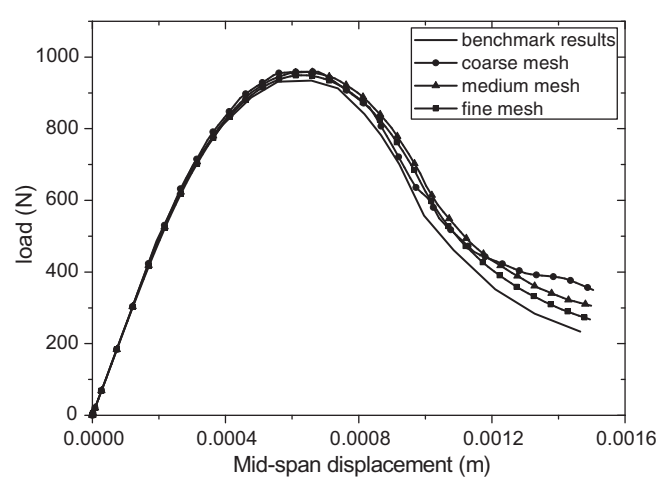

Fig. 12. Mesh independent load–displacement responses using consistent microscopic cell.

degradation of continua can be characterized from the Helmholtz free energy. Under this framework, a unified approach for numerical characterization of a class of damage evolution functions has been proposed. It is shown that this energy equivalence relationship is consistent with that obtained from asymptotic based homogenization, and it serves as an energy bridging vehicle between the damaged continuum and cracked microstructure.

Please cite this article in press as: Ren, X., et al. Micro-cracks informed damage models for brittle solids. Int. J. Solids Struct. (2011), doi:10.1016/j.ijsolstr.2011.02.001

Fig. 13. Contour of normal stress in horizontal direction.

Fig. 14. Contour of normal strain in horizontal direction.

It is shown that the damage evolution functions characterized by the microscopic cell with energy bridging exhibit a strong numerical size effect identical to the physical size effect reported in the literature. We attribute this to the critical value of crack opening displacement which does not scale with the overall dimension of the microscopic cell and the specimen. Approaches without this consideration, such as the conventional continuum damage models, yield a strong mesh dependency in the numerical solution. The proposed method with energy bridging allows for proper scaling of the damage evolution functions to eliminate this mesh dependency in the continuum solution.

In this approach, the microscopic cell analysis is used to obtain the homogenized stress–strain curves associated with fundamental damage modes for characterization of the macroscopic damage evolution functions through energy bridging. The numerical example of a three-point bending test with Mode I fracture is considered due to the available experimental data for comparison with the numerical prediction. For more general and complex loading histories, including those that could yield heterogeneous failure processes where different damage modes exist at different macroscopic points, one needs to consider (1) the appropriate macroscopic damage model suitable for describing the complex damage mechanisms (with the most complete model being the fully tensorial damage model), and (2) the corresponding microscopic cell analyses sufficient for characterizing each of the damage evolution functions associated with the damage model parameters. Practically, especially for the most general tensorial damage model, these whole processes add considerable complexities into the computational framework, and this calls for further research investigation.

The proposed method can be used as a means for numerical characterization of damage evolution functions that have been traditionally done by experimentation. This approach can also be used as the enhancement of continuum damage mechanics with embedded microstructure properties for a wide range of solids containing arbitrary crack configurations and microstructures. These will be the extension of the present work, and the results are to be reported in the forthcoming publications.

Acknowledgements

Financial support from the US Army Engineer Research and Development Center (Grant No. W912HZ-07-C-0019) to UCLA and National Science Foundation of China for key Project (Grant No. 90715033) to Tongji University is gratefully acknowledged. Permission to publish was granted by Director, Geotechnical & Structures Laboratory.

Appendix A. Derivation of influence tensor using asymptotic expansion based homogenization

An alternative approach for relating microscopic and macroscopic variables is the asymptotic expansion based homogenization method. Consider the model problem described by coarse-scale coordinate $\mathbf{x}$ and fine-scale coordinate $\mathbf{y}$ as shown in Fig. 1. The two length scales are related with a small parameter, ε, as

$$\mathbf{y} = \frac{1}{\varepsilon}\mathbf{x} \tag{A.1}$$

The spatial derivatives of a function Φ^{ε} with superscript ε denoting the combined (total) coarse-fine scale characters is expressed as

$$\nabla_{\mathbf{x}}\Phi^{\varepsilon}(\mathbf{x}) = \nabla_{\mathbf{x}}\Phi(\mathbf{x},\mathbf{y}) = \nabla_{\mathbf{x}}\Phi(\mathbf{x},\mathbf{y}) + \frac{1}{\varepsilon}\nabla_{\mathbf{y}}\Phi(\mathbf{x},\mathbf{y}) \tag{A.2}$$

Based on asymptotic expansion, the total displacement vector is expanded as

$$\mathbf{u}^{\varepsilon}(\mathbf{x}) = \sum_{i=0}^{\infty}\varepsilon^{i}\mathbf{u}^{[i]}(\mathbf{x},\mathbf{y}) \tag{A.3}$$

Substituting (A.3) into Eq. (6) and considering (A.1) and (A.2), we obtain expansion of the strain tensor as

$$\mathbf{e}^{\varepsilon} = \nabla^{s}_{\mathbf{x}}\mathbf{u}^{\varepsilon} = \sum_{k=-1}^{\infty}\varepsilon^{k}\mathbf{e}^{[k]} \tag{A.4}$$

where

$$\mathbf{e}^{[-1]} = \nabla^{s}_{\mathbf{y}}\mathbf{u}^{[0]} \tag{A.5}$$

$$\mathbf{e}^{[k]}(u) = \nabla^{s}_{\mathbf{x}}\mathbf{u}^{[k]} + \nabla^{s}_{\mathbf{y}}\mathbf{u}^{[k+1]} \quad k \geqslant 0 \tag{A.6}$$

Introducing the elasticity tensor, we have the stress expansion as follows

$$\boldsymbol{\sigma}^{\varepsilon} = \mathbf{C}^{\varepsilon} : \mathbf{e}^{\varepsilon} = \sum_{k=-1}^{\infty}\varepsilon^{k}\boldsymbol{\sigma}^{[k]} \tag{A.7}$$

where

$$\boldsymbol{\sigma}^{[k]} = \mathbf{C}^{\varepsilon} : \mathbf{e}^{[k]} \tag{A.8}$$

Substituting expansion (A.8) into the equilibrium condition in Eq. (1), we obtain the leading order equilibrium equations

$$\nabla_{\mathbf{y}} \cdot \boldsymbol{\sigma}^{[-1]} = 0 \tag{A.9}$$

$$\nabla_{\mathbf{x}} \cdot \boldsymbol{\sigma}^{[k]} + \nabla_{\mathbf{y}} \cdot \boldsymbol{\sigma}^{[k+1]} = 0, \quad k \geqslant -1 \tag{A.10}$$

The formal solutions of these equations have been discussed in the literature (Guedes and Kikuchi, 1990; Cheng, 1992; Fish et al., 1997, etc.), and here we only outline the important results. The first and second order formal solutions for displacement are expressed as

$$\mathbf{u}^{[0]} = \mathbf{v}^{[0]}(\mathbf{x}) \tag{A.11}$$

$$\mathbf{u}^{[1]} = \mathbf{v}^{[1]}(\mathbf{x}) + \boldsymbol{\chi}(\mathbf{y}) : \nabla^s_{\mathbf{x}} \mathbf{v}^{[0]}(\mathbf{x}) \tag{A.12}$$

where $\mathbf{v}^{[0]}(\mathbf{x})$ and $\mathbf{v}^{[1]}(\mathbf{x})$ are the coarse and fine-scale solution functions of $\mathbf{u}$, and $\boldsymbol{\chi}$ ($\mathbf{y}$) is the third order characteristic tensor function of the microscopic cell (Bakhvalov and Panasenko, 1989).

Consider the truncation of the strain and stress expansions to two scales:

$$\mathbf{e}^{\varepsilon} = \frac{1}{\varepsilon}\mathbf{e}^{[-1]} + \mathbf{e}^{[0]} + \cdots \approx \frac{1}{\varepsilon}\mathbf{e}^{[-1]} + \mathbf{e}^{[0]} \tag{A.13}$$

$$\boldsymbol{\sigma}^{\varepsilon} = \frac{1}{\varepsilon}\boldsymbol{\sigma}^{[-1]} + \boldsymbol{\sigma}^{[0]} + \cdots \approx \frac{1}{\varepsilon}\boldsymbol{\sigma}^{[-1]} + \boldsymbol{\sigma}^{[0]} \tag{A.14}$$

where

$$\mathbf{e}^{[-1]} = \nabla^s_{\mathbf{y}} \mathbf{u}^{[0]} = \nabla^s_{\mathbf{y}} \mathbf{v}^{[0]}(\mathbf{x}) = 0 \tag{A.15}$$

$$\boldsymbol{\sigma}^{[-1]} = \mathbf{C}^{\varepsilon} : \mathbf{e}^{[-1]} = \mathbf{C}^{\varepsilon} : \nabla^s_{\mathbf{y}} \mathbf{u}^{[0]} = \mathbf{C}^{\varepsilon} : \nabla^s_{\mathbf{y}} \mathbf{v}^{[0]}(\mathbf{x}) = 0 \tag{A.16}$$

$$\mathbf{e}^{[0]} = \nabla^s_{\mathbf{x}} \mathbf{u}^{[0]} + \nabla^s_{\mathbf{y}} \mathbf{u}^{[1]} = \left[\mathbf{I} + \nabla^s_{\mathbf{y}} \boldsymbol{\chi}(\mathbf{y})\right] : \nabla^s_{\mathbf{x}} \mathbf{v}^{[0]}(\mathbf{x}) \tag{A.17}$$

$$\boldsymbol{\sigma}^{[0]} = \mathbf{C}^{\varepsilon} : \mathbf{e}^{[0]} = \mathbf{C}^{\varepsilon} : \left[\mathbf{I} + \nabla^s_{\mathbf{y}} \boldsymbol{\chi}(\mathbf{y})\right] : \nabla^s_{\mathbf{x}} \mathbf{v}^{[0]}(\mathbf{x}) \tag{A.18}$$

Substituting (A.15)–(A.18) into (A.13), (A.14), we have

$$\mathbf{e}^{\varepsilon} \approx \mathbf{e}^{[0]} = \nabla^s_{\mathbf{x}} \mathbf{u}^{[0]} + \nabla^s_{\mathbf{y}} \mathbf{u}^{[1]} = [\mathbf{I} + \nabla^s_{\mathbf{y}} \boldsymbol{\chi}(\mathbf{y})] : \nabla^s_{\mathbf{x}} \mathbf{u}^{[0]}(\mathbf{x}) \tag{A.19}$$

$$\boldsymbol{\sigma}^{\varepsilon} \approx \boldsymbol{\sigma}^{[0]} = \mathbf{C}^{\varepsilon} : [\mathbf{I} + \nabla^s_{\mathbf{y}} \boldsymbol{\chi}(\mathbf{y})] : \nabla^s_{\mathbf{x}} \mathbf{u}^{[0]}(\mathbf{x}) \tag{A.20}$$

where $\mathbf{I}$ denotes the fourth order identity tensor. Substituting stress expression (A.20) into equilibrium equation (1) and the cohesive traction equation. (4), we have the following equations for solving the third order tensor $\boldsymbol{\chi}(\mathbf{y})$

$$\nabla_{\mathbf{y}} \cdot \left(\mathbf{C}^{\varepsilon} : \nabla^s_{\mathbf{y}} \boldsymbol{\chi}(\mathbf{y})\right) = 0 \quad \text{in } \Omega_y \tag{A.21}$$

$$[\mathbf{C}^{\varepsilon} : \nabla^s_{\mathbf{y}} \boldsymbol{\chi}(\mathbf{y}) : \nabla^s_{\mathbf{x}} \mathbf{v}^{[0]}(\mathbf{x})] \cdot \mathbf{n} = -[\mathbf{C}^{\varepsilon} : \nabla^s_{\mathbf{x}} \mathbf{v}^{[0]}(\mathbf{x})] \cdot \mathbf{n} + \mathbf{h} \quad \text{on } \Gamma_c \tag{A.22}$$

Comparing Eqs. (17) and (A.19), the influence tensor can be expressive by the characteristic tensor:

$$\mathbf{A}^{\varepsilon} = -\nabla^s_{\mathbf{y}} \boldsymbol{\chi}(\mathbf{y}) \tag{A.23}$$

Appendix B. Derivation of energy bridging equation using asymptotic expansion based homogenization

Here we show that the energy bridging Eq. (34) can be obtained by the asymptotic expansion based method. Substituting Eqs. (A.19) and (A.20) into the microscopic free energy defined in Eq. (29) yields

$$\begin{aligned}\Psi^{\varepsilon} &= \tfrac{1}{2}\boldsymbol{\sigma}^{\varepsilon} : \mathbf{e}^{\varepsilon} = \tfrac{1}{2}\mathbf{e}^{\varepsilon} : \mathbf{C}^{\varepsilon} : \mathbf{e}^{\varepsilon} = \tfrac{1}{2}\left(\nabla^s_{\mathbf{x}} \mathbf{u}^{[0]} + \nabla^s_{\mathbf{y}} \mathbf{u}^{[1]}\right) : \mathbf{C}^{\varepsilon} \\ &: \left(\nabla^s_{\mathbf{x}} \mathbf{u}^{[0]} + \nabla^s_{\mathbf{y}} \mathbf{u}^{[1]}\right) = \tfrac{1}{2}\nabla^s_{\mathbf{x}} \mathbf{u}^{[0]} : \mathbf{C}^{\varepsilon} : \nabla^s_{\mathbf{x}} \mathbf{u}^{[0]} + \tfrac{1}{2}\nabla^s_{\mathbf{y}} \mathbf{u}^{[1]} : \mathbf{C}^{\varepsilon} \\ &: \nabla^s_{\mathbf{y}} \mathbf{u}^{[1]} + \nabla^s_{\mathbf{x}} \mathbf{u}^{[0]} : \mathbf{C}^{\varepsilon} : \nabla^s_{\mathbf{y}} \mathbf{u}^{[1]}\end{aligned} \tag{B.1}$$

Integrating over the microscopic cell, we obtain

$$\begin{aligned}\int_{\Omega_Y} \Psi^{\varepsilon}\, d\Omega &= \int_{\Omega_Y} \left(\frac{1}{2}\nabla^s_{\mathbf{x}} \mathbf{u}^{[0]} : \mathbf{C}^{\varepsilon} : \nabla^s_{\mathbf{x}} \mathbf{u}^{[0]}\right) d\Omega \\ &+ \int_{\Omega_Y} \left(\frac{1}{2}\nabla^s_{\mathbf{y}} \mathbf{u}^{[1]} : \mathbf{C}^{\varepsilon} : \nabla^s_{\mathbf{y}} \mathbf{u}^{[1]}\right) d\Omega \\ &+ \int_{\Omega_Y} \left(\nabla^s_{\mathbf{x}} \mathbf{u}^{[0]} : \mathbf{C}^{\varepsilon} : \nabla^s_{\mathbf{y}} \mathbf{u}^{[1]}\right) d\Omega\end{aligned} \tag{B.2}$$

The three terms on the right hand side of Eq. (B.2) are rearranged as follows. The first term is expressed as

$$\int_{\Omega_Y} \left(\frac{1}{2}\nabla^s_{\mathbf{x}} \mathbf{u}^{[0]} : \mathbf{C}^{\varepsilon} : \nabla^s_{\mathbf{x}} \mathbf{u}^{[0]}\right) d\Omega = \frac{V_y}{2}\nabla^s_{\mathbf{x}} \mathbf{u}^{[0]} : \langle \mathbf{C}^{\varepsilon} \rangle : \nabla^s_{\mathbf{x}} \mathbf{u}^{[0]} \tag{B.3}$$

The second term can be further manipulated by considering $k = -1$ in Eq. (A.10) to yield:

$$\nabla_{\mathbf{x}} \cdot \boldsymbol{\sigma}^{[-1]} + \nabla_{\mathbf{y}} \cdot \boldsymbol{\sigma}^{[0]} = 0 \quad \text{in } \Omega_y \tag{B.4}$$

Further considering the crack surface traction condition

$$\boldsymbol{\sigma}^{[0]} \cdot \mathbf{n} = \mathbf{h} \quad \text{on } \Gamma_c \tag{B.5}$$

Substituting Eq. (A.16) in Eq. (B.4), we have

$$\nabla_{\mathbf{y}} \cdot \boldsymbol{\sigma}^{[0]} = 0 \tag{B.6}$$

Multiplying Eq. (B.6) by $\mathbf{u}^{[1]}$ and integrating it over Ω_y yields

$$\int_{\Omega_Y} \mathbf{u}^{[1]} \cdot \nabla_{\mathbf{y}} \cdot \boldsymbol{\sigma}^{[0]}\, d\Omega = 0 \tag{B.7}$$

By integration by parts, we have

$$\begin{aligned}\int_{\Omega_Y} \mathbf{u}^{[1]} \cdot \nabla_{\mathbf{y}} \cdot \boldsymbol{\sigma}^{[0]}\, d\Omega &= \int_{\Omega_Y} \boldsymbol{\sigma}^{[0]} \cdot \nabla_{\mathbf{y}} \cdot \mathbf{u}^{[1]}\, d\Omega - \int_{\Gamma_c} \mathbf{u}^{[1]} \cdot \boldsymbol{\sigma}^{[0]} \\ &\cdot \mathbf{n}\, dS \\ &= 0\end{aligned} \tag{B.8}$$

where Γ_c is the crack surface within the microscopic cell. Considering the boundary condition in Eq. (B.5) and the symmetry of stress tensor, $\boldsymbol{\sigma}^{[0]}$, we have

$$\int_{\Omega_Y} \boldsymbol{\sigma}^{[0]} : \nabla^s_{\mathbf{y}} \mathbf{u}^{[1]}\, d\Omega = -\int_{\Gamma_c} \mathbf{u}^{[1]} \cdot \mathbf{h}\, dS \tag{B.9}$$

Substituting Eq. (A.18) into Eq. (B.9), one obtains

$$\begin{aligned}\int_{\Omega_Y} \nabla^s_{\mathbf{x}} \mathbf{u}^{[0]} : \mathbf{C}^{\varepsilon} : \nabla^s_{\mathbf{y}} \mathbf{u}^{[1]}\, d\Omega + \int_{\Omega_Y} \nabla^s_{\mathbf{y}} \mathbf{u}^{[1]} : \mathbf{C}^{\varepsilon} : \nabla^s_{\mathbf{y}} \mathbf{u}^{[1]}\, d\Omega \\ = -\int_{\Gamma_c} \mathbf{u}^{[1]} \cdot \mathbf{h}\, dS\end{aligned} \tag{B.10}$$

The second term on the right side of Eq. (B.2) is then obtained. For the third term on the right hand side of Eq. (B.2), considering Eq. (A.12):

$$\begin{aligned}\int_{\Omega_Y} \nabla^s_{\mathbf{x}} \mathbf{u}^{[0]} : \mathbf{C}^{\varepsilon} : \nabla^s_{\mathbf{y}} \mathbf{u}^{[1]}\, d\Omega = \nabla^s_{\mathbf{x}} \mathbf{u}^{[0]} : \left[\int_{\Omega_Y} \mathbf{C}^{\varepsilon} : \nabla^s_{\mathbf{y}} \boldsymbol{\chi}(\mathbf{y})\, d\Omega\right] \\ : \nabla^s_{\mathbf{x}} \mathbf{u}^{[0]}\end{aligned} \tag{B.11}$$

Substituting Eq. (A.20) into the homogenized stress expressed in Eq. (14) yields

$$\begin{aligned}\bar{\boldsymbol{\sigma}} = \langle \boldsymbol{\sigma}^{\varepsilon} \rangle = \left\langle \mathbf{C}^{\varepsilon} : \left[\mathbf{I} + \nabla^s_{\mathbf{y}} \boldsymbol{\chi}(\mathbf{y})\right] \right\rangle : \nabla^s_{\mathbf{x}} \mathbf{u}^{[0]}(\mathbf{x}) = \langle \mathbf{C}^{\varepsilon} \rangle \\ : \nabla^s_{\mathbf{x}} \mathbf{u}^{[0]}(\mathbf{x}) + \langle \mathbf{C}^{\varepsilon} : \nabla^s_{\mathbf{y}} \boldsymbol{\chi}(\mathbf{y}) \rangle : \nabla^s_{\mathbf{x}} \mathbf{u}^{[0]}(\mathbf{x})\end{aligned} \tag{B.12}$$

Comparing Eq. (B.11) with (B.12) gives

$$V_y \bar{\boldsymbol{\sigma}} : \nabla^s_{\mathbf{x}} \mathbf{u}^{[0]} = V_y \nabla^s_{\mathbf{x}} \mathbf{u}^{[0]} : \langle \mathbf{C}^{\varepsilon} \rangle : \nabla^s_{\mathbf{x}} \mathbf{u}^{[0]} + \int_{\Omega_Y} \nabla^s_{\mathbf{x}} \mathbf{u}^{[0]} : \mathbf{C}^{\varepsilon} : \nabla^s_{\mathbf{y}} \mathbf{u}^{[1]}\, d\Omega \tag{B.13}$$

Then substituting Eqs. (B.3), (B.10) and (B.13) into Eq. (B.2), we obtain

$$\frac{1}{V_y}\left(\int_{\Omega_Y}\Psi^{\varepsilon}\,\mathrm{d}\Omega+\frac{1}{2}\int_{\Gamma_c}\mathbf{u}^{[1]}\cdot\mathbf{h}\,\mathrm{d}S\right)=\frac{1}{2}\bar{\boldsymbol{\sigma}}:\nabla^s_{\mathbf{x}}\mathbf{u}^{[0]} \tag{B.14}$$

It is observed that $\nabla^s_{\mathbf{x}}\mathbf{u}^{[0]}$ is the macroscopic strain, $\bar{\mathbf{e}}$, which is imposed on the microscopic cell by Eq. (32). By substituting Eq. (25) in Eq. (B.14), we finally obtain

$$\overline{\Psi}=\frac{1}{V_y}\left(\int_{\Omega_Y}\Psi^{\varepsilon}\,\mathrm{d}\Omega+\frac{1}{2}\int_{\Gamma_c}\mathbf{u}^{[1]}\cdot\mathbf{h}\,\mathrm{d}S\right) \tag{B.15}$$

Appendix C. Two-variable damage model

According to the continuum damage theory, the general expression of the fourth order damage representation is

$$\boldsymbol{\sigma}=(\mathbf{I}-\mathbf{D}):\mathbf{C}_0:\boldsymbol{\varepsilon}^e \tag{C.1}$$

where $\mathbf{C}_0$ is the initial elastic stiffness tensor, $\mathbf{D}$ is the fourth order damage tensor, and $\boldsymbol{\varepsilon}^e=\boldsymbol{\varepsilon}-\boldsymbol{\varepsilon}^p$and $\boldsymbol{\varepsilon}_p$ is the plastic strain. The effective stress is defined as

$$\boldsymbol{\sigma}_0=\mathbf{C}_0:\boldsymbol{\varepsilon}^e \tag{C.2}$$

Hence the damage model in (C.1) can be expressed as

$$\boldsymbol{\sigma}=(\mathbf{I}-\mathbf{D}):\boldsymbol{\sigma}_0 \tag{C.3}$$

To account for the unilateral effect, the positive-negative decomposition of the effective stress tensor is defined as follows

$$\boldsymbol{\sigma}_0=\boldsymbol{\sigma}_0^+ + \boldsymbol{\sigma}_0^- \tag{C.4}$$

$$\boldsymbol{\sigma}_0^+=\mathbf{P}^+:\boldsymbol{\sigma}_0 \tag{C.5}$$

$$\boldsymbol{\sigma}_0^-=\boldsymbol{\sigma}_0-\boldsymbol{\sigma}_0^+=\mathbf{P}^-:\boldsymbol{\sigma}_0 \tag{C.6}$$

where the fourth order projection tensors $\mathbf{P}^+$ and $\mathbf{P}^-$ are (Faria et al., 1998):

$$\mathbf{P}^+=\sum_i H(\hat{\sigma}_i)\mathbf{p}_i\otimes\mathbf{p}_i\otimes\mathbf{p}_i\otimes\mathbf{p}_i \tag{C.7}$$

$$\mathbf{P}^-=\mathbf{I}-\mathbf{P}^+ \tag{C.8}$$

in which $\mathbf{I}$ is the fourth order identity, $\hat{\sigma}_i$ and $\mathbf{p}_i$ are the ith eigenvalue and the corresponding eigenvector for the effective stress tensor $\boldsymbol{\sigma}_0$, and $H(\cdot)$ is the Heaviside function:

$$H(x)=\begin{cases}1 & x\geqslant 0\\ 0 & x<0\end{cases} \tag{C.9}$$

Correspondingly, two damage scalars, d^+ and d^-, are introduced to describe the damage of materials under tension and compression respectively. According to the thermodynamics, the state of an ensemble could be described by using the definition of Helmholtz free energy (HFE), which is expressed by using the state variables and internal variables. We define the total elastoplastic HFE as

$$\psi=\psi(\boldsymbol{\varepsilon}^e,\boldsymbol{\kappa},d^+,d^-) \tag{C.10}$$

where $\boldsymbol{\kappa}$ is plastic variables. Decomposing the total HFE into the elastic and the plastic components, we have

$$\psi(\boldsymbol{\varepsilon}^e,\boldsymbol{\kappa},d^+,d^-)=\psi^e(\boldsymbol{\varepsilon}^e,d^+,d^-)+\psi^p(\boldsymbol{\varepsilon}^e,\boldsymbol{\kappa},d^+,d^-) \tag{C.11}$$

Neglecting the plastic strain under tension, we have the following plastic HFE

$$\psi^p(\boldsymbol{\varepsilon}^e,\boldsymbol{\kappa},d^+,d^-)=\psi^p(\boldsymbol{\varepsilon}^e,\boldsymbol{\kappa},d^-)=(1-d^-)\psi_0^p \tag{C.12}$$

The elastic HFE is further decomposed as

$$\begin{aligned}\psi^e(\boldsymbol{\varepsilon}^e,d^+,d^-)&=\psi^{e+}(\boldsymbol{\varepsilon}^e,d^+)+\psi^{e+}(\boldsymbol{\varepsilon}^e,d^-)\\&=(1-d^+)\psi_0^{e+}(\boldsymbol{\varepsilon}^e)+(1-d^-)\psi_0^{e-}(\boldsymbol{\varepsilon}^e)\end{aligned} \tag{C.13}$$

Here the superscripts "e" and "p" refer to "elastic" and "plastic" components, respectively, and the subscript "0" refers to the "initial" state.

According to the second principle of thermodynamics, the following equation is obtained

$$\boldsymbol{\sigma}=\frac{\partial\psi^e}{\partial\boldsymbol{\varepsilon}^e}=(1-d^+)\boldsymbol{\sigma}_0^+ + (1-d^-)\boldsymbol{\sigma}_0^- = (\mathbf{I}-d^+\mathbf{P}^+ - d^-\mathbf{P}^-):\boldsymbol{\sigma}_0 \tag{C.14}$$

The damage energy release rate (DERR) can then be obtained as

$$Y^{\pm}=\frac{\partial\psi}{\partial d^{\pm}} \tag{C.15}$$

References

Abaqus 6.5 user's manual, 2005.
Bakhvalov, N., Panasenko, G., 1989. Homogenization: Averaging Processes in Periodic Media. Kluwer Academic Publishers Group, Dordrecht.
Bazant, Z.P., 1984. Size effect in blunt fracture: concrete, rock, metal. J. Eng. Mech., ASCE 110 (4), 518–535.
Belytschko, T., Loehnert, S., Song, JH., 2008. Multiscale aggregating discontinuities: a method for circumventing loss of material stability. Int. J. Numer. Methods Mech. Eng. 73, 869–894.
Benssousan, A., Lions, J.L., Papanicolaou, G., 1978. Asymptotic Analysis for Periodic Media. North-Holland, Armsterdam.
Budiansky, B., O'connell, R.J., 1976. Elastic moduli of cracked solid. Int. J. Solids Struct. 12, 81–95.
Chen, J.S., Pan, C.H., Tu, C.T., Liu, W.K., 1996. Reproducing kernel particle methods for large deformation analysis of non-linear structures. Comput. Methods Appl. Mech. Eng. 139, 195–227.
Cheng, C.H., 1992. Modeling of the elasto-plastic behavior for composite materials using homogenization method. Ph.D. dissertation, University of Michigan, MI.
Dascalu, C., Bilbie, G., Agiasofitou, E.K., 2008. Damage and size effects in elastic solids: a homogenization method. Int. J. Solids Struct. 45, 409–430.
Dascalu, C., 2009. A two-scale damage model with material length. Comptes Rendus Mécanique 337 (9-10), 645–652.
de Borst, R., 1986. Ph.D. thesis, Delft University of Technology, The Netherlands.
Faria, R., Oliver, J., Cervera, M., 1998. A strain-based plastic viscous-damage model for massive concrete structures. Int. J. Solids Struct. 35 (14), 1533–1558.
Fish, J., Shek, K., Pandheeradi, M., Shephard, M.S., 1997. Computational plasticity for composite structures based on mathematical homogenization: theory and practice. Comput. Methods Appl. Mech. Eng. 148 (1-2), 53–73.
Fish, J., Yu, Q., Shek, K., 1999. Computational damage mechanics for composite materials based on mathematical homogenization. Int. J. Numer. Methods Eng. 45, 1657–1679.
Fleming, M., Chu, Y.A., Moran, B., Belyschko, T., 1997. Enriched element-free Garlerkin methods for crack tip fields. Int. J. Numer. Methods Eng. 40, 1483–1504.
Guedes, J.M., Kikuchi, N., 1990. Preprocessing and postprocessing for materials based on the homogenization method with adaptive finite element methods. Comput. Methods Appl. Mech. Eng. 83 (2), 143–198.
Ju, J.W., 1989. On energy-based coupled elastoplastic damage theories: constitutive modeling and computational aspects. Int. J. Solids Struct. 25 (7), 803–833.
Hashin, Z., 1988. The differential scheme and its application to cracked materials. J. Mech. Phys. Solids 36, 719–734.
Hill, R., 1963. Elastic properties of reinforced solids: some theoretical principles. J. Mech. Phys. Solids. 11, 357–372.
Kachanov, L.M., 1958. On creep rupture time. Izv. Akad. Nauk. 8, 26–31.
Lee, K., Moorthy, S., Ghosh, S., 1999. Multiple scale computational model for damage in composite materials. Comput. Methods Appl. Mech. Eng. 172, 175–201.
Lemaitre, J., Chaboche, J.L., 1974. A nonlinear model of creep-fatigue damage cumulation and interaction. In: Proceeding of TUTAM Symposium of Mechanics of Visco-elasticity Media and Bodies. Springer-Verlag, Gotenbourg, Sweden.
Li, J., Ren, X.D., 2009. Stochastic damage model for concrete based on energy equivalent strain. Int. J. Solids Struct. 46, 2407–2419.
Liu, W.K., Jun, S., Zhang, Y.F., 1995. Reproducing kernel particle methods. Int. J. Numer. Methods Fluids 20, 1081–1106.
Mazars, J., 1984. Application de la mecanique de l'endommangement au comportement non lineaire et a la rupture du beton de structure. These de Doctorate d'Etat, L.M.T., Universite Paris, France.
Meyer, R., Ahrens, H., Duddeck, H., 1994. Material model for concrete in cracked and uncracked states. J. Eng. Mech. Div., ASCE 120 (9), 1877–1895.
Möes, N., Belytschko, T., 2002. Extended finite element method for cohesive crack growth. Eng. Fract. Mech. 69, 813–833.
Mori, T., Tanaka, K., 1973. Average stress in matrix and average elastic energy of materials with misfitting inclusions. Acta Metall. 21, 571–583.
Nemat-Nasser, S., Hori, M., 1999. Micromechanics: Overall Properties of Heterogeneous Materials, 2nd ed. Elsevier Science B.V.
Norris, A.N., 1985. A different scheme for the effective moduli of composites. Mech. Mater. 4, 1–16.

Petersson, P.E., 1981. Crack Growth and Development of Fracture Zones in Plain Concrete and Similar Materials. Report No. TVBM-1006, Division of Building Materials, University of Lund, Sweden.

Robotnov, Y.N., 1968. Creep rupture. Appl. Mech., Proc. ICAM-12, 342–349.

Wu, J.Y., Li, J., Faria, R., 2006. An energy release rate-based plastic-damage model for concrete. Int. J. Solids Struct. 43 (3–4), 583–612.

Please cite this article in press as: Ren, X., et al. Micro-cracks informed damage models for brittle solids. Int. J. Solids Struct. (2011), doi:10.1016/j.ijsolstr.2011.02.001